High-Speed Tracking of a Nanopositioning Stage Using Modified Repetitive Control

Chun-Xia Li, *Student Member, IEEE*, Guo-Ying Gu, *Member, IEEE*, Mei-Ju Yang, *Student Member, IEEE*, and Li-Min Zhu, *Member, IEEE*

***Abstract*—In this paper, a modified repetitive control (MRC) based approach is developed for high-speed tracking of nanopositioning stages. First, the hysteresis nonlinearity is decomposed as a periodic disturbance over a linear system. Then, the MRC technique is utilized to account for the periodic disturbances/errors caused by the hysteresis and dynamics behaviors. The developed approach provides a simple and effective hysteresis compensation strategy, avoiding the constructions of hysteresis model and its inversion. Besides, with improved loop-shaping properties, the MRC can alleviate the nonperiodic disturbance amplification problem of the conventional repetitive control. Finally, the effectiveness and performance of the developed MRC-based approach are verified by the experimental results on a custom-built piezo-actuated stage in terms of hysteresis compensation, disturbance rejection and tracking accuracy.**

***Note to Practitioners*—High-speed piezo-actuated nanopositioning stages are playing an increasingly important role in the fields of scanning probe microscopes (SPMs). However, the tracking speed and accuracy of the nanopositioning stages are hindered by the hysteresis and dynamics behaviors of the piezo-actuated systems. In this work, a MRC-based approach is developed, which is tailored for the lateral scanning process of SPMs. The MRC can directly mitigate the hysteresis by decomposing it as a periodic disturbance, which releases the burden of hysteresis model construction. Besides, the MRC has a better nonperiodic disturbance rejection capability than the conventional repetitive control. Experimental results demonstrate the merits of the MRC-based approach in terms of hysteresis compensation, disturbance rejection, and tracking accuracy. Due to a simple structure and ease of implementation, the developed MRC-based approach can be applied to other piezo-actuated nanopositioning systems involving with the hysteresis.**

***Index Terms*—Hysteresis compensation, modified repetitive control, nanopositioning stage, piezoelectric actuator, tracking control.**

I. Introduction

With the development of nanotechnology, nanopositioning stages are widely used in many high-precision positioning and tracking applications, such as scanning probe microscopes (SPMs) [1], ultra-precision machine tools [2], and nano-manipulation [3]. Recently, besides high-precision positioning, high-bandwidth operation of nanopositioning stages are increasingly required in the fields of high-speed SPMs [4], [5] and high-throughput nanomanufacturing [6].

Most nanopositioning stages employ piezoelectric stack actuators (PSAs) for actuation owing to their advantages of ultra-high resolution, fast response time, and large stiffness [7], [8]. However, the inherent hysteresis nonlinearity of the PSAs and the vibrational dynamics behaviors of the stages lead to the control challenges for the piezo-actuated nanopositioning stages [9], [8]. To mitigate the hysteresis nonlinearity, many control approaches have been investigated in the literature, such as charge control [10], inverse-model feedforward control [11], closed-loop feedback control [12], and combined feedforward-feedback control [13]. To deal with the vibrational dynamics, various vibration control techniques are developed [14], [15]. The readers may refer to [9] for an overview of the control strategies for nanopositioning systems. It is worthy of mentioning that during high-speed tracking the hysteresis nonlinearity and the vibrational dynamics are usually coupled to affect the tracking performance [16], which makes it more challenging to develop effective controllers for the nanopositioning stages.

Note that in many applications, for instance, the lateral scanning process of SPMs, the reference trajectories of the nanopositioning stages are periodic [17], [18] and the tracking errors caused by the hysteresis and dynamics behaviors are also periodic [18]. Therefore, repetitive control (RC) [19] which is tailored for periodic operation has attracted a mount of research efforts in such applications [18], [20]–[26]. As a learning-type control strategy, RC can effectively reduce the tracking errors with the increase of the operation periods. Quite often, the repetitive controller can be plugged into an existing feedback control loop to improve the tracking performance of the system [18], [19], [24], which is ease of implementation. Hence, RC is promising in the tracking control of piezo-actuated nanopositioning stages. However, the commonly used RC is a control strategy based on linear systems [19], [26] and the hysteresis nonlinearity of the PSAs in nanopositioning stages limits its direct implementation. To address such issue, one common approach is to mitigate the hysteresis nonlinearity with a feedforward inverse hysteresis compensator (IHC) and then RC can be implemented, as reported in [21]–[23] and [26]. However, due to the complexity of the hysteresis nonlinearity, it is generally not a simple task to construct the hysteresis model and its inversion. Moreover, the feedforward IHC also complicates the control structure and implementation. As an alternative approach, in [18] and [24], the hysteresis nonlinearity is considered to be mitigated by the existing feedback controller and then

Manuscript received March 25, 2015; accepted April 27, 2015. This paper was recommended for publication by Associate Editor Y. Zhang and Editor Y. Sun upon evaluation of the reviewers' comments. This work was supported in part by the National Natural Science Foundation of China under Grant 51325502 and Grant 51405293, and in part by the Specialized Research Fund for the Doctoral Program of Higher Education under Grant 20130073110037.

The authors are with State Key Laboratory of Mechanical System and Vibration, School of Mechanical Engineering, Shanghai Jiao Tong University, Shanghai 200240, China (e-mail: lichunxia@sjtu.edu.cn; guguoying@sjtu.edu.cn; yangmeixianglian@sjtu.edu.cn; zhulm@sjtu.edu.cn).

Color versions of one or more of the figures in this paper are available online at http://ieeexplore.ieee.org.

Digital Object Identifier 10.1109/TASE.2015.2428437

RC is applied for the linearized system. However, in these applications, the tracking frequencies are generally low (5–25 Hz), where the hysteresis nonlinearity is not so complicated as that of high frequencies.

Although RC has been widely applied in nanopositioning stages [18], [20]–[26], there is still an issue not considered in these applications. As is known, RC is an approach based on internal model principle [27], where a signal generator is integrated in the feedback loop to provide high gains at the harmonics of the reference trajectory [19]. Such high gains offer the capability for RC to track periodic trajectory. However, in the conventional repetitive control (CRC), the enhanced performance at the periodic frequencies commonly results in deteriorated loop shapes at other frequencies [28]. In other words, undesired gain amplifications usually occur at other nonperiodic frequencies. When the plant is subjected to nonperiodic disturbances, the tracking performance with CRC will be deteriorated [28]. In the literature, this problem is not considered or addressed during the application of CRC in the nanopositioning stages [18], [20]–[26], where high precision is generally important and necessary.

In this paper, a modified repetitive control (MRC) based approach is developed for high-speed tracking of piezo-actuated nanopositioning stages with periodic reference inputs. The MRC strategy was proposed by Chen and Tomizuka [28] for linear dynamics systems. To the best knowledge of the authors, this work is the first attempt at introducing the MRC technique for the high-speed tracking control of nanopositioning stages involving with the complicated hysteresis nonlinearity. The distinctive characteristics of this work are as follows.

i) It is theoretically analyzed that for periodic reference input the hysteresis nonlinearity can be decomposed as a bounded periodic disturbance over a linear system. Then, the MRC strategy is introduced to handle the hysteresis nonlinearity by rejecting the periodic disturbance. Its effectiveness is validated by real-time experiments in a wide frequency range, especially at high frequencies. In this sense, the constructions of the hysteresis model and its inversion are avoided. This significantly reduces the implementation complexity compared to the CRC-based control approaches with IHCs as in [21]–[23] and [26]. Therefore, this paper provides an alternative option, which is novel, simple and effective, to deal with hysteresis nonlinearity of piezo-actuated nanopositining stages.

ii) With improved loop-shaping properties, the MRC can alleviate the nonperiodic disturbance amplification problem of CRC [18], [20]–[24]. Thus, the MRC can achieve better tracking performance in terms of tracking accuracy and disturbance rejection as compared to CRC, which is experimentally demonstrated. Such improvement is of great significance for nanopositioning stages since high precision is generally important and necessary in their applications.

iii) The rigorous stability and robust stability of the MRC are analyzed in detail and an optimization approach is presented for the parameter determination of the MRC, which provides an option to select more appropriate parameters of the MRC. Due to a simple structure and ease of implementation, the presented control approach can also be applied to other piezo-actuated nanopositioning systems.

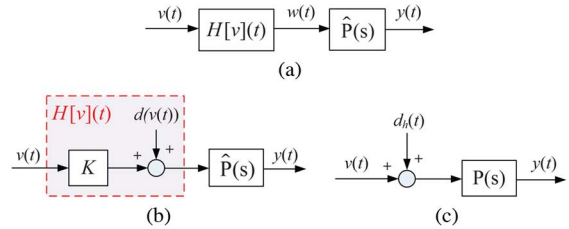

Fig. 1. Decomposition of the hysteresis nonlinearity. (a) System with hysteresis nonlinearity. (b) Decomposition of the hysteresis nonlinearity. (c) Equivalent schematic diagram of (b).

The remainder of this paper is organized as follows. The design of the MRC-based control approach are presented in Section II. In Section III, the experimental setup, controller implementation and controller performance analysis are presented. Experiments are performed in Section IV, followed by the conclusion in Section V.

II. MRC-Based Control Approach Design

In this section, the MRC-based control approach for tracking control of piezo-actuated nanopositioning stages is developed. First, it is theoretically analyzed that for periodic reference input the hysteresis nonlinearity can be decomposed as a bounded periodic disturbance over a linear system. Then, the design of MRC strategy is presented. Finally, the rigorous stability and robust stability conditions are analyzed and an optimization approach is presented for the parameters determination of MRC.

A. Hysteresis Decomposition

As analyzed in Section I, the hysteresis nonlinearity of the PSAs makes it challenging for precision tracking control of the nanopositioning stages. In this work, we try to find a method to mitigate the hysteresis nonlinearity with available control approaches instead of constructing the inverse hysteresis model.

Generally, the hysteresis nonlinearity can be denoted as the following operator:

$$w(t) = H[v](t) \tag{1}$$

where $w(t)$ is the hysteresis output, usually unmeasurable, and $v(t)$ is the input voltage to the PSA, as shown in Fig. 1(a). The relation between $w(t)$ and the output displacement of the piezo-actuated stage $y(t)$ is described by a linear time-invariant system $\widehat{P}(s)$.

Following the derivation in [29], the hysteresis can be expressed as a linear gain K and a bounded nonlinear term $d(v(t))$ satisfying $|d(v(t))| \leq \rho := \sup_{t\geq 0} |d(v(t))|$ as follows:

$$w(t) = H[v](t) = Kv(t) + d\left(v(t)\right) \tag{2}$$

with

$$d\left(v(t)\right) = (w_0 - Kv_0)e^{-\alpha(v-v_0)\mathrm{sgn}(\dot{v})} + e^{-\alpha v \mathrm{sgn}(\dot{v})} \int_{v_0}^{v} (b-K)e^{\alpha\tau\mathrm{sgn}(\dot{v})} d\tau \tag{3}$$

where v is the abbreviation of $v(t)$, $\dot{v}$ is the abbreviation of $\dot{v}(t)$, $\omega_0 = \omega(0)$, $v_0 = v(0)$, α and b are constants related to the hysteresis nonlinearity. Then, the whole system can be expressed as Fig. 1(b). For a periodic input $v(t)$ with a period of T, it is obvious that $v(t+T) = v(t)$ and $\dot{v}(t+T) = \dot{v}(t)$. Then, with these relations and (3), it can be gotten that $d(v(t+T)) = d(v(t))$, i.e., $d(v(t))$ is periodic.

From an input–output perspective, the whole system can be further decomposed as a linear time-invariant system $P(s) = K\widehat{P}(s)$ with a bounded input disturbance $d_h(t) = d(v(t))/K$, as shown in Fig. 1(c). For a periodic reference input $v(t)$, it is straightforward that $d_h(t+T) = d(v(t+T))/K = d(v(t))/K = d_h(t)$, i.e., the disturbance $d_h(t)$ caused by the hysteresis nonlinearity can also be treated as periodic. Then, the periodic disturbance $d_h(t)$ can be directly mitigated by the MRC strategy developed in the following sections.

B. MRC Design

RC is an effective control strategy to track periodic references and reject periodic disturbances. However, the commonly used RC only applies to linear systems [19], [26]. The hysteresis nonlinearity of the PSAs limits its direct application to nanopositioning stages. In this work, due to the hysteresis decomposition in Section II-A, the system can be regarded as a linear one with a bounded periodic disturbance. Therefore, the RC can be developed for the piezo-actuated nanopositioning stages involving with hysteresis nonlinearity.

Conceptually speaking, RC is designed based on the internal model principle [27]. In CRC, a generalized periodic signal generator $1/(1-z^{-N})$ (N is the sampling number in each period of the reference input) is introduced in the repetitive control loop to provide high gains at the harmonics of the reference trajectory [19], which offers the capability for CRC to track periodic trajectory. However, such characteristic is along with undesired gain amplifications at other frequencies, which means that the nonperiodic disturbances/errors are amplified [28]. Unfortunately, such disadvantage is inevitable for CRC which uses the signal generator $1/(1-z^{-N})$.

In this work, a MRC strategy proposed by Chen and Tomizuka [28] is adopted, which can alleviate the nonperiodic disturbance amplification problem of CRC. The essential feature of the MRC is the employment of a spectrum-selection filter to extract only the periodic components of the tracking errors for the feedback control in the repetitive control loop, which improves the loop-shaping properties of MRC as compared to CRC. Fig. 2 shows the block diagram of the MRC for a linear system $P(z)$, where $C(z)$ represents an existing feedback controller, $P_{\mathrm{ZPET}}(z)$ is a stable approximate model inversion of the plant $P(z)$ derived using the Zero-Phase-Error-Tracking (ZPET) algorithm [30], z^{-m} is a delay term related to the plant and model inversion which satisfies $z^{-m} \approx P_{\mathrm{ZPET}}(z)P(z)$, $Q(z)$ is the spectrum-selection filter. $Q(z)$ also plays a role of counteracting the m-step delay of the input signals to it. It should be mentioned that the periodic disturbance $d_h(k)$ resulting from the hysteresis is included in the input disturbance $d_i(k)$.

It is worthy of noting that the MRC strategy is also intended to mitigate the hysteresis nonlinearity by rejecting the periodic disturbance $d_h(k)$. In this sense, the constructions of the hysteresis model and inversion are avoided, which significantly reduces the implementation complexity as compared to the previous CRC-based control approaches with the IHCs [21]–[23], [26].

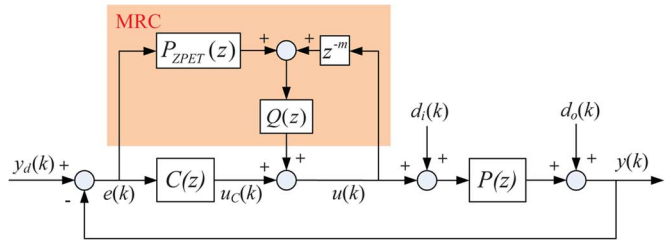

Fig. 2. The block diagram of the control approach using the MRC technique.

It can be observed from Fig. 2 that the MRC can be plugged into the control system to improve the tracking performance while the existing feedback controller $C(z)$ remains unchanged, which is ease of implementation. Another advantage is that the MRC and $C(z)$ can be designed independently. Here, the MRC is designed first. Without loss of generality, the dynamics of the system $P(z)$ can be expressed as

$$P(z) = z^{-d}\frac{B(z)}{A(z)} = z^{-d}\frac{B_s(z)B_u(z)}{A(z)} \tag{4}$$

where d denotes the relative degree of $P(z)$, $B_s(z)$ contains all the stable zeros and $B_u(z)$ contains all the unstable zeros. Then, the model inversion $P_{\mathrm{ZPET}}(z)$ using the ZPET technique [30] is obtained as

$$P_{\mathrm{ZPET}}(z) = z^{-(nc+nu)}\frac{A(z)B_u^f(z)}{B_s(z)\left(B_u(1)\right)^2} \tag{5}$$

where $B_u^f(z)$ is derived by flipping the polynomial coefficients of $B_u(z)$, nu is the order of $B_u(z)$ and nc is the delays added to keep $P_{\mathrm{ZPET}}(z)$ causal. Obviously, $nc = O(A(z)B_u^f(z)) - O(z^{nu}B_s(z)) = nu$. Considering that $z^{-m} \approx P_{\mathrm{ZPET}}(z)P(z)$, m is derived as

$$m = d + nc = d + nu \tag{6}$$

Then, the spectrum-selection filter $Q(z)$ is designed as [28]

$$Q(z) = \frac{(1-\beta)z^{-(N-m)}}{1-\beta z^{-N}},\ \beta \in [0,1) \tag{7}$$

where β is the parameter to generate loop shapes different from the CRC.

Finally, the sensitivity function $S(z)$, i.e. the transfer function from the reference input $y_d(k)$ to the tracking error $e(k)$, can be obtained as

$$\begin{aligned} S(z) &= \frac{1-z^{-m}Q(z)}{1+P(z)C(z)+\left(P(z)P_{\mathrm{ZPET}}(z)-z^{-m}\right)Q(z)} \\ &\approx \frac{1-z^{-m}Q(z)}{1+P(z)C(z)} \end{aligned} \tag{8}$$

It is obvious from (8) that the MRC affects the baseline feedback system with $C(z)$ by the numerator $1-z^{-m}Q(z)$. With (7), the numerator of $S(z)$ can be written as

$$1-z^{-m}Q(z) = \frac{1-z^{-N}}{1-\beta z^{-N}}. \tag{9}$$

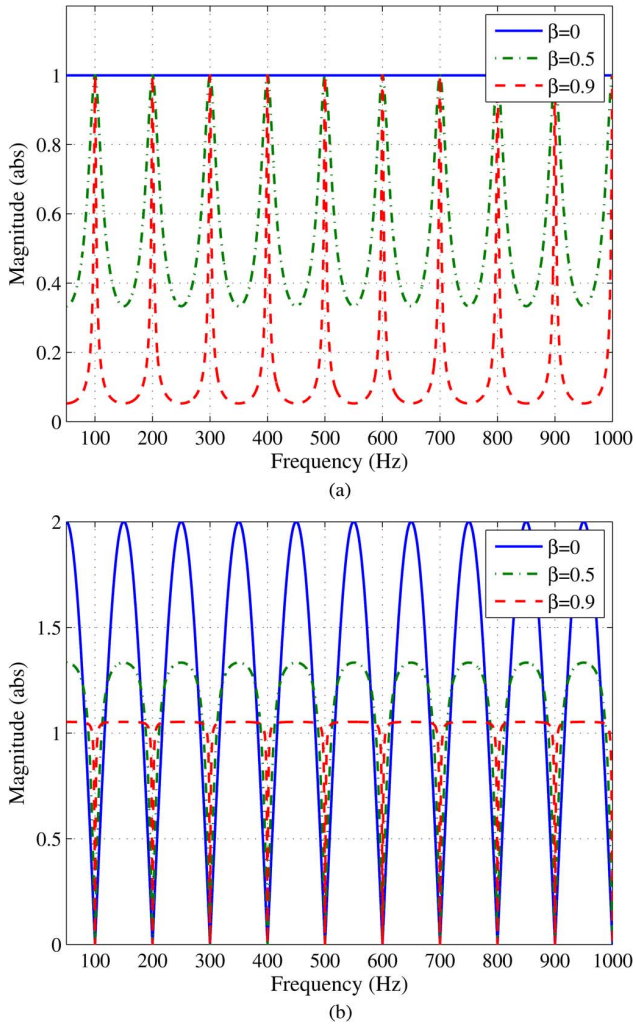

Fig. 3. Magnitude responses of $Q(z)$ and $1-z^{-m}Q(z)$ with different values of β. Here, the low-pass filter $q(z,z^{-1})$ is not incorporated in $Q(z)$. $N=500$, $m=5$, and $T_s=0.00002\ s$ are used as an illustrative example, where T_s is the sampling time interval of the system. (a) $Q(z)$. (b) $1-z^{-m}Q(z)$.

To investigate how β affects the performance of $Q(z)$ and the MRC, the magnitude responses of $Q(z)$ and $1-z^{-m}Q(z)$ with different values of β are plotted in Fig. 3(a). Specially, if $\beta=0$, we can arrive at $1-z^{-m}Q(z)=1-z^{-N}$ and the MRC generates a loop shape similar to the CRC. As can be seen from Fig. 3, the magnitude of $Q(z)$ when $\beta=0$ is always 1, which means that both periodic and nonperiodic components can pass $Q(z)$ to generate the feedback control input. At the same time, the maximum value of $1-z^{-m}Q(z)$ at unexpected frequencies is 2, which means that some nonperiodic disturbances are inevitably amplified by 100%. On the contrary, if β is given a large value close to 1, the magnitude of $Q(z)$ is 1 only at the repetitive frequencies. Thus, $Q(z)$ can be regarded as a spectrum-selection filter to extract the periodic components. Correspondingly, the amplification of nonperiodic disturbance is much reduced with the increase of β. In particular, the maximum value of $1-z^{-m}Q(z)$ with $\beta=0.9$ is only 1.053 (much lower than 2), which validates that the MRC alleviates the nonperiodic disturbance amplification problem of CRC. As there always exist nonperiodic disturbances in practical applications, e.g., the ambient noise and impulse noise, the MRC tends to achieve better tracking performances in terms of tracking accuracy and disturbance rejection as compared to the CRC, which will be experimentally demonstrated in the Section IV. It should be noted that such improvement is of great significance for nanopositioning stages since high precision is important and necessary in their applications.

As the MRC provides high-gain control at high frequencies, it may excite the unmodeled dynamics of the plant and introduce potential closed-loop instability in the application. Therefore, a zero-phase low-pass filter $q(z,z^{-1})$ is introduced in $Q(z)$ as

$$q(z,z^{-1})=(az^{-1}+b+az)^i \tag{10}$$

where a and b satisfy $2a+b=1$, and i is a positive integer. Although $q(z,z^{-1})$ is noncausal, the delay terms $z^{-(N-m)}$ in $Q(z)$ makes $q(z,z^{-1})$ applicable. Therefore, the finally implemented $Q(z)$ can be expressed as

$$Q(z)=\frac{(1-\beta)z^{-(N-m-n_q)}}{1-\beta z^{-N}}z^{-n_q}q(z,z^{-1}) \tag{11}$$

where n_q is the delay term to make $q(z,z^{-1})$ causal.

C. Baseline Feedback Controller

To develop the baseline controller $C(z)$, as shown in Fig. 2, various control approaches, such as proportional-integral-derivative control [7], H_∞ control [24], sliding mode control [31], and control strategy based on modern control theory [32] can be adopted. Among these approaches, the most commonly used method in commercial SPMs is the integral or proportional-integral (PI) control [10] due to the advantages of simple implementation and robustness to modeling errors. Therefore, in this work, the PI controller is utilized as the baseline feedback controller. The transfer function of the discrete-time PI controller is $C(z)=K_p+K_iT_s/(z-1)$, where K_p and K_i are the proportional and integral gains, respectively.

D. Stability and Robust stability

In this section, the conditions for stability and robust stability of the closed-loop system are analyzed, which will provide significant insight in the controller design process and give criterion for the determination of the controller parameters. The stability condition and robust stability condition and their proofs are provided as follows.

Theorem 1 (Stability): Assume that the closed-loop system with feedback controller $C(z)$ is asymptotically stable, i.e. $1+P(z)C(z)=0$ has no roots outside the unit circle in the z-plane. If the low-pass filter $q(z,z^{-1})$ fulfill the following condition:

$$\left|q(z,z^{-1})\right|_{z=e^{j\omega T_s}}<\left|\frac{1+P(z)C(z)}{P(z)P_{\mathrm{ZPET}}(z)-z^{-m}}\right|_{z=e^{j\omega T_s}} \tag{12}$$

for $\omega\in[0,\pi/T_s]$, then the closed-loop system with the MRC, as shown in Fig. 2, is asymptotically stable.

Proof: First, the closed-loop transfer function from the reference input $y_d(k)$ to the output $y(k)$ is derived as

$$T(z)=\frac{P(z)C(z)+P(z)P_{\mathrm{ZPET}}(z)Q(z)}{1+P(z)C(z)+\left(P(z)P_{\mathrm{ZPET}}(z)-z^{-m}\right)Q(z)}. \tag{13}$$

Thus, the characteristic polynomial of the closed-loop system can be expressed as

$$\begin{aligned} D(z) &= 1 + P(z)C(z) + \left(P(z)P_{\mathrm{ZPET}}(z) - z^{-m}\right) Q(z) \\ &= (1 + P(z)C(z)) \\ &\quad \times \left(1 + \frac{\left(P(z)P_{\mathrm{ZPET}}(z) - z^{-m}\right) Q(z)}{1 + P(z)C(z)}\right) \end{aligned} \tag{14}$$

where $(1 + P(z)C(z))$ is stable by the assumption. Therefore, the stability of the closed-loop system with the MRC depends on the second term on the right-hand side in (14). According to the Small Gain Theorem [33], we obtain the stability condition

$$\left| \frac{\left(P(z)P_{\mathrm{ZPET}}(z) - z^{-m}\right) Q(z)}{1 + P(z)C(z)} \right|_{z=e^{j\omega T_s}} < 1 \tag{15}$$

for $\omega \in [0, \pi/T_s]$. It can be found that (15) is satisfied if the following condition is met:

$$|Q(z)|_{z=e^{j\omega T_s}} < \left| \frac{1 + P(z)C(z)}{P(z)P_{\mathrm{ZPET}}(z) - z^{-m}} \right|_{z=e^{j\omega T_s}} \tag{16}$$

with $\omega \in [0, \pi/T_s]$.

If we denote $\widehat{Q}(z) = (1-\beta)z^{-(N-m)}/(1-\beta z^{-N})$, it can be easily obtained that $|\widehat{Q}(z)|_{z=e^{j\omega T_s}} \leq 1$. Then, the following condition holds:

$$\begin{aligned} |Q(z)| &= \left|\widehat{Q}(z)q(z, z^{-1})\right| \\ &\leq \left|\widehat{Q}(z)\right| \left|q(z, z^{-1})\right| \\ &\leq \left|q(z, z^{-1})\right| \end{aligned} \tag{17}$$

for $z = e^{j\omega T_s}$ and $\omega \in [0, \pi/T_s]$. Combining (16) with (17), it can be derived that the closed-loop system with the MRC is stable when condition (12) is satisfied. ■

Remark 1:

1) As the characteristic polynomial of the closed-loop transfer functions from $d_i(k)$ to $y(k)$ and from $d_o(k)$ to $y(k)$ are the same with (14), the stability condition (12) is general.
2) It can be found from (12) that the value of β does not affect the stability of the closed-loop system. What is directly related to the system stability is the low-pass filter $q(z, z^{-1})$. Therefore, $q(z, z^{-1})$ should be appropriately designed.

Theorem 2 (Robust Stability): Let the plant be modeled as $\widetilde{P}(z) = P(z)(1+\Delta_p(z))$. Assume that the nominal model $P(z)$ can be stabilized by the feedback controller $C(z)$ and the MRC, i.e., (12) is satisfied. Then, the closed-loop system has robust stability if the model uncertainty $\Delta_p(z)$ satisfies

$$|\Delta_p(z)|_{z=e^{j\omega T_s}} < 1/\left|T(z)\right|_{z=e^{j\omega T_s}} \tag{18}$$

for $\omega \in [0, \pi/T_s]$, where $T(z)$ is given in (13).

Proof: From (14), the characteristic polynomial of the closed-loop system with plant $\widetilde{P}(z)$ can be expressed as (the z-domain index is omitted for the sake of simplicity)

$$\begin{aligned} \widetilde{D}(z) &= 1 + P(1+\Delta_p)C + \left(P(1+\Delta_p)P_{\mathrm{ZPET}} - z^{-m}\right) Q \\ &= \left(1 + PC + (PP_{\mathrm{ZPET}} - z^{-m})Q\right) \\ &\quad \times \left(1 + \frac{PC + PP_{\mathrm{ZPET}}Q}{1 + PC + (PP_{\mathrm{ZPET}} - z^{-m})Q}\Delta_p\right) \\ &= D(1 + T\Delta_p) \end{aligned} \tag{19}$$

where D is stable by assumption. Thus, to guarantee the robust stability of the closed-loop system, $(1 + T\Delta_p)$ must be stable. With the Small Gain Theorem [33], we can arrive at a sufficient condition for the robust stability of the system

$$|T\Delta_p| \leq |T||\Delta_p| < 1. \tag{20}$$

Then, the robust stability condition (18) can be easily derived. ■

E. Controller Parameters Optimization

From the above analysis, it can be found that the low-pass filter $q(z, z^{-1})$ has a significant effect on the performance of the MRC. When a low cutoff frequency of $q(z, z^{-1})$ is chosen, the stability condition and robust stability condition are easier to be satisfied. However, since $q(z, z^{-1})$ also reduces the control gains of the MRC, a low cutoff frequency can not guarantee the tracking accuracy at high frequencies. Due to the contradiction between the stability and tracking performance of MRC, the determination of the parameters of $q(z, z^{-1})$ becomes challenging. In this work, to select appropriate parameters for $q(z, z^{-1})$, an optimization approach is proposed. The maximum optimization problem with constraints can be formulated as follows:

$$\begin{aligned} &\max_{a,b,i} \omega_c \\ &s.t. \\ &\begin{cases} 2a + b = 1 \\ i \in \mathbb{N}_+ \\ q(z, z^{-1}) = (az^{-1} + b + az)^i \\ \left|q(z, z^{-1})\right|_{z=e^{j\omega_c T_s}} = 0.707 \\ \left|q(z, z^{-1})\right| < |L_s| \\ |\Delta_p(z)| < |L_r| \\ \left|q(z, z^{-1})\right|_{z=e^{j\omega_h T_s}} \leqslant \lambda \end{cases} \end{aligned} \tag{21}$$

where ω_c is the cutoff frequency of $q(z, z^{-1})$, $L_s = (1 + P(z)C(z))/(P(z)P_{\mathrm{ZPET}}(z) - z^{-m})$ is the stability bound in (12) and $L_r = 1/T(z)$ is the robust stability bound in (18). The first constraint is aimed at keeping a unity DC gain for the low-pass filter $q(z, z^{-1})$. The last constraint is intended to ensure the roll off of $q(z, z^{-1})$ at high frequencies, which contributes to reducing the influence of high-frequency noise. This constraint is achieved by limiting the allowable maximum magnitude λ at the frequency of ω_h. As can be observed, the optimization is intended to maximize the cutoff frequency of $q(z, z^{-1})$ on the basis that the conditions for stability and robust stability are satisfied. Thus, the tracking performance is enhanced to the maximum extent.

Remark 2: In this work, the controller parameters are determined by a systematic way: i) the conditions for stability and robust stability are firstly analyzed and ii) based on these conditions, the parameters of the low-pass filter are determined by an optimization approach. This is different from that in [28], where the stability condition is not given and there are no rules or criterion for the selection of the low-pass filter parameters.

III. Controller Implementation and Performance Analysis

In this section, the experimental setup is established firstly. Then, the dynamic model of the piezo-actuated nanopositioning stage is identified. Based on the identified model, the control

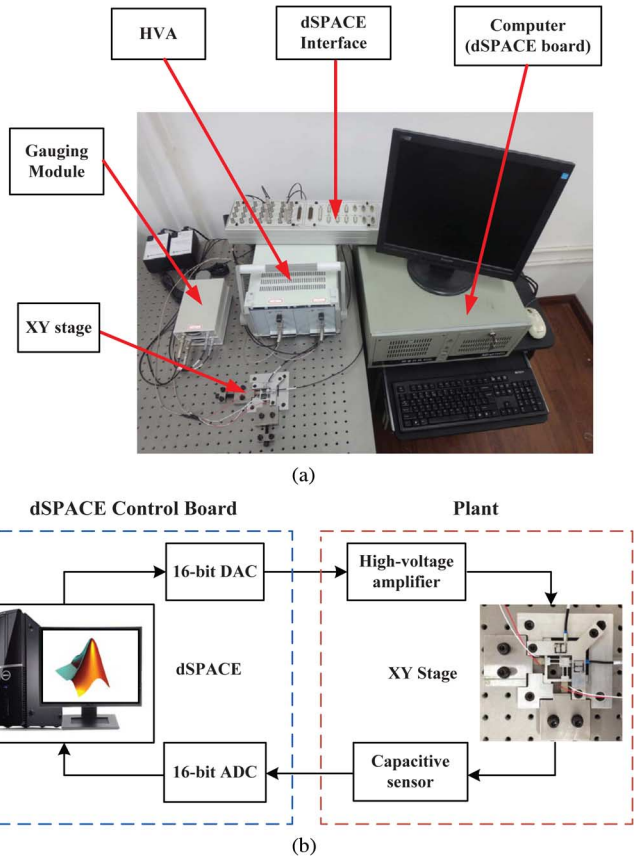

Fig. 4. The experimental setup. (a) The experimental platform. (b) Block diagram of the experimental platform.

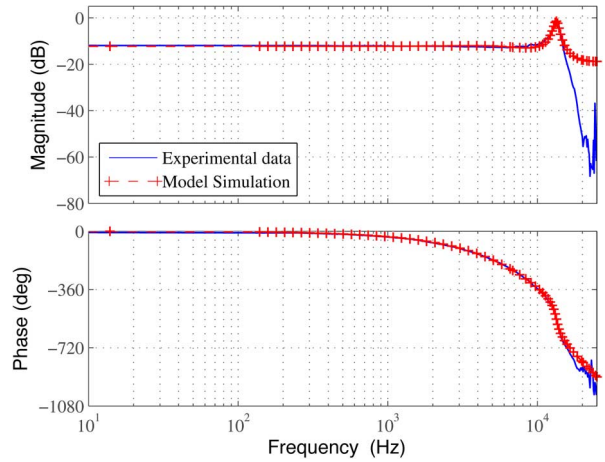

Fig. 5. Comparison of frequency responses of experimental results and model simulation results.

approach developed in Section II is implemented and the controller performance is analyzed.

A. Experimental Setup

In this work, a piezo-actuated XY nanopositioning stage designed in our previous work [34] is adopted to evaluate the developed MRC-based control approach. The piezo-actuated stage has high resonance frequencies over 13.6 kHz, which makes it possible to verify the effectiveness of the MRC-based control approach in a wide frequency range. It is worthy of mentioning that the piezo-actuated stage is well decoupled [34], and thus the two-axis motions can be treated independently. For the purpose of verifying the developed control approach, only the treatment of X-axis tracking control is presented in this work.

The experimental platform is shown in Fig. 4. A dSPACE-DS1103 board equipped with the 16-bit analog to digital converters (ADCs) and 16-bit digital to analog converters (DACs) is utilized to implement real-time control laws in the Matlab/Simulink environment. The DACs produce analog control input (0–10 V) and a dual-channel high-voltage amplifier (HVA) with a fixed gain of 20 is used to provide excitation voltage (0–200 V) for the PSAs (Noliac NAC 2021-H12). Capacitive sensors (Probe 2823 and Gauging Module 8810 from MicroSense, range of $+/-25$ μm with analog output of $+/-10$ V) are adopted to measure the displacements of the end-effector of the stage. The sensor output signals corresponding to the real-time displacement information are then captured by the ADCs for feedback control. In this work, the sampling frequency of the system is set to 50 kHz. The block diagram of the whole experimental setup is shown in Fig. 4(b).

Remark 3: The capacitive sensors used here are readjusted by the manufacturer to extend the measuring range to $+/-25$ μm, as the original small measuring range ($+/-10$ μm) restricts their use for other stages. Therefore, the output range of the sensors is different from that in [34]. Additionally, the range extension makes measuring accuracy of the sensors a little worse than that in [34].

B. System Identification

Due to the hysteresis decomposition in Section II-A, the nanopositioning system can be regarded as a linear system with a bounded input disturbance. According to the discussion in Section II-B, the dynamic model of the linear system should be identified firstly in order to design the MRC strategy. For this purpose, a band-limited white noise signal with low amplitude is used to excite the system. The low amplitude is intended to minimize the effect of the hysteresis [24]. Then, the System Identification Toolbox of Matlab is adopted to identify the dynamic model which can be expressed as

$$P(z) = z^{-1} \times \frac{0.0094(z^2 + 0.5351z + 2.561)}{(z^2 - 0.8756z + 0.2821)} \times \frac{(z^2 - 4.552z + 8.908)}{(z^2 + 0.208z + 0.8655)}. \quad (22)$$

Fig. 5 shows the comparison of the frequency responses of the system (blue solid line) and the identified model (red dashed line with marker) to demonstrate the effectiveness of the identification. It can be seen that the identified model captures the dynamics of the system in a wide frequency range with sufficient accuracy.

C. Controller Implementation

As discussed in Section II-B, the parameters of the PI controller and MRC can be determined independently. Hence, the parameters of the PI controller are first determined. The proportional gain K_p and the integral gain K_i are initially selected by

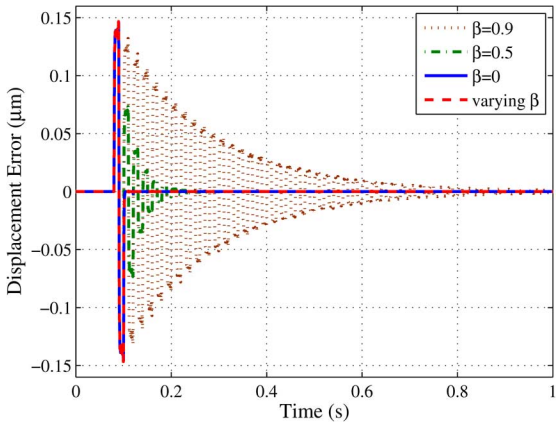

Fig. 6. Simulation results of the tracking errors under 50-Hz triangular trajectory using MRC with different values of β.

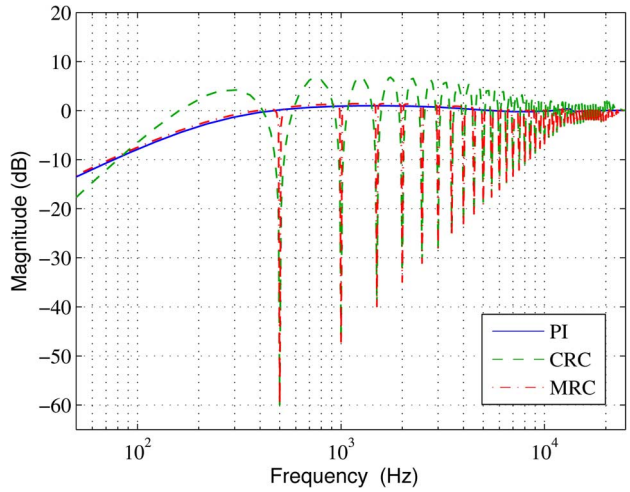

Fig. 7. Bode plot of sensitivity function with different controllers.

the simulation in Matlab/Simulink, and then tuned by the trial and error method as $K_p = 0.1$ and $K_i = 6000$. The parameters of MRC are determined based on the identified linear dynamic model in (22) using the following steps.

1) P_{ZPET} is obtained by (5) and the parameter m is derived with (6).
2) The low-pass filter $q(z, z^{-1})$ is determined with a cutoff frequency of 9.1 kHz by the optimization presented in Section II-E.
3) For the selection of β, simulation of tracking a 50-Hz triangular trajectory with different values of β is carried out.

The simulation results are shown in Fig. 6. As can be seen, the smaller value of β results in the faster convergence of the tracking error. However, smaller value of β also leads to larger amplification of nonperiodic disturbances according to the analysis in Section II-B. In order to achieve both fast error convergence and good nonperiodic disturbance rejection performance, a time-varying β is adopted. The value of β is set as 0 for the first 2.5 cycle to achieve fast error convergence, then linearly increased to 0.9 for the 2.5-to-4.5 cycle, and finally kept constant at 0.9. The performance of the time-varying β is also evaluated in Fig. 6. As can be seen, the error convergence with the time-varying β is as fast as that with $\beta = 0$.

D. Controller Performance Analysis

Before the tracking experiments are conducted, the controller performance is investigated by analyzing the sensitivity function $S(z)$ in (8). The magnitude response of $S(z)$ is shown in Fig. 7. It should be noted that the magnitude response is plotted with $N = 100$ as an illustrative example which corresponds to a tracking frequency of 500 Hz. As can be seen, with the MRC, deep notches appear at the frequencies of multiples of 500 Hz which indicates that the errors at such frequencies are eliminated. During periodic trajectory tracking, since the tracking errors caused by hysteresis and dynamics behaviors are accounted for, the MRC can improve the tracking speed and accuracy compared with the PI control. Additionally, it can be observed from Fig. 7 that the magnitude of these notches gradually decreases as the frequencies increase, which reduces the compensation capacity of the MRC at high frequencies. This is due to the employment of low-pass filter in $Q(z)$ as analyzed in Section II-E.

To compare the performance of the MRC with the CRC, the sensitivity function with CRC [19], [23], [24] is also plotted in Fig. 7. It can be observed that the loop shapes of $1 - z^{-m}Q(z)$ ($\beta = 0$) at nonperiodic frequencies, as illustrated in Fig. 3(b), are preserved here, which means that large amplification of nonperiodic errors is unavoidable with CRC. By contrast, it can be observed from the figure that the loop shapes of MRC at nonperiodic frequencies are nearly the same with the PI controller, much lower than those of the CRC. Therefore, the MRC can alleviate the nonperiodic disturbance amplification problem of the CRC and it tends to have a better disturbance rejection capability in the practical applications, which coincides with the analysis in Section II-B.

IV. Experimental Results

In this section, comparative experiments are performed on the piezo-actuated nanopositioning stage to evaluate the performance of the developed MRC-based control approach in trajectory tracking, hysteresis compensation and disturbance rejection.

A. Open-Loop Hysteresis

The open-loop tests of the piezo-actuated nanopositioning stage are firstly conducted with triangular signal inputs at different frequencies. Fig. 8 shows the experimental results, which illustrates the input–output relationship. As can be observed, the nanopositioning stage shows severe hysteresis nonlinearity in the open-loop strategy. The hysteresis nonlinearity caused errors (h/H), as shown in Fig. 8, become more serious with the increase of the input frequencies. It can also be seen from the figure that the hysteresis loops become more complex at high input frequencies, which is due to the coupling effect of the hysteresis nonlinearity and dynamics behaviors. This makes it more challenging to develop effective controllers for high-speed tracking of the nanopositioning stage. The effectiveness of the developed MRC-based control approach on the hysteresis compensation will be verified in the following experiments.

B. Tracking Performance and Hysteresis Compensation

1) Tracking Performance: To verify the effectiveness of the developed MRC-based control approach on the tracking

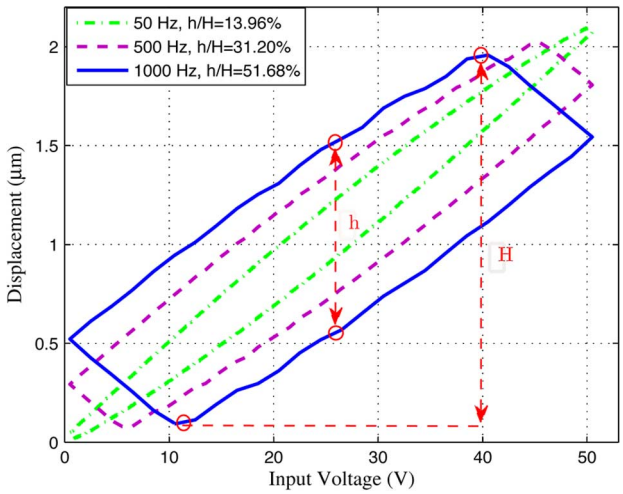

Fig. 8. Open-loop hysteresis of the piezo-actuated stage with triangular signal inputs at different frequencies.

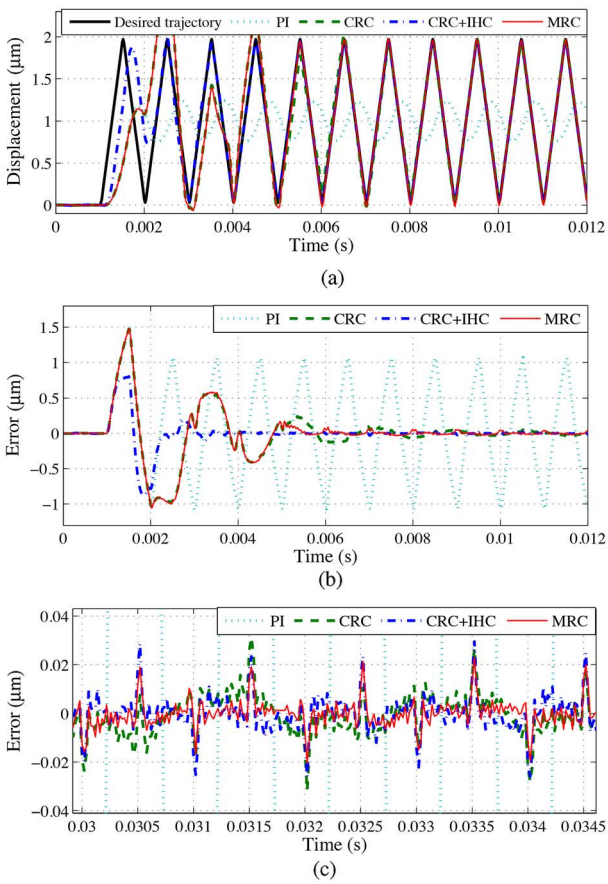

Fig. 9. Experimental results of tracking 1000-Hz triangular trajectory using PI control, CRC, CRC+IHC, and MRC. (a) Tracking results. (b) Tracking error. (c) The detail of steady-state tracking error.

performance improvement as compared to PI control and CRC [19], [23], [24], experiments are performed on the piezo-actuated stage under triangular trajectories with frequencies of 50, 500, and 1000 Hz. It should be noted that these triangular trajectories are constructed using the first seven odd harmonics. As an illustration, Fig. 9 shows the experimental results of tracking 1000-Hz triangular trajectory. From the figure, it can

TABLE I
STEADY-STATE TRACKING ERRORS OF DIFFERENT CONTROLLERS UNDER TRIANGULAR TRAJECTORIES WITH DIFFERENT FREQUENCIES

		PI	CRC	CRC+IHC	MRC
50 Hz	$e_{\max}$ (nm)	128.0	9.9	9.3	6.8
	e_{rms} (nm)	98.3	2.7	2.9	2.1
500 Hz	$e_{\max}$ (nm)	923.6	10.9	11.1	10.7
	e_{rms} (nm)	610.3	2.8	3.0	2.8
1000 Hz	$e_{\max}$ (nm)	1074.8	33.5	32.8	27.2
	e_{rms} (nm)	660.8	7.6	7.7	6.2

be seen that the tracking performance with the developed MRC strategy is significantly better than that with PI control. It can also be observed from the detail of steady-state tracking error, as shown in Fig. 9(c), that the MRC-based control approach improves the steady-state tracking performance of CRC. This is further evidenced in Table I, which summarizes the steady-state maximum tracking error $(e_{\max})$ and root-mean-square tracking error $(e_{\rm rms})$. It should be noted that such improvement is of great significance for nanopositioning stages since high precision is important and necessary in their applications. In addition, it can be observed from Table I that the tracking accuracy of the MRC-based control approach falls down as the tracking frequency increases. This is caused by the low-pass filter $q(z, z^{-1})$, which has been discussed in Sections II-E and III-D. Nevertheless, high-speed tracking up to 1000 Hz with high accuracy is achieved with the MRC.

Remark 4: The advantage of the developed MRC compared with the CRC is that the MRC can alleviate the nonperiodic disturbance amplification problem of CRC, which may be caused by the ambient noise during experiments. In fact, if the ambient noise (especially the noise at the frequency where it would be amplified by the CRC) is not severe, the difference of the tracking performance with the MRC and CRC may be not obvious. Therefore, the experimental result with MRC as summarized in Table I is slightly better than CRC, and for 500-Hz trajectory MRC gives almost the same result as CRC.

To further evaluate the performance of the MRC-based control approach, comparative experiments with the CRC+IHC are also conducted, where the IHC is developed based on a modified Prandtl-Ishlinskii model proposed in our previous work [35]. In fact, the IHC is a direct inverse hysteresis model which can be described as $v(t) = a_1 y_d^3(t) + a_2 y_d(t) + \sum_{i=1}^{N} p_i F_{r_i}[y_d](t)$, where a_1 and a_2 are constants, p_i denotes the weighting value of the play operator with the threshold value r_i, and N is the number of the play operators. The readers may refer to [35] for detailed discussions. In this work, ten play operators $(N = 10)$ is chosen for the parameter identification with the threshold values r_i determined as $r_i = i/N\|y_d(t)\|_\infty$, $i = 0, 1, 2, \ldots, N-1$ with $\|y_d(t)\|_\infty = 1$ in the normalized cases. The parameters are identified as $a_1 = 0.07854$, $a_2 = 1.84775$, $p_1 = -0.54368$, $p_2 = -0.34002$, $p_3 = -0.00040$, $p_4 = -0.15387$, $p_5 = -0.03567$, $p_6 = 0$, $p_7 = -0.02908$, $p_8 = -0.04996$, $p_9 = -0.10365$, and $p_{10} = -0.25510$. After cascading the IHC in the feedforward path of the piezo-actuated stage, a new linear system model is identified for the design of CRC. Then, experiments of tracking triangular trajectories using CRC+IHC are carried out. The experimental result is also shown in Fig. 9.

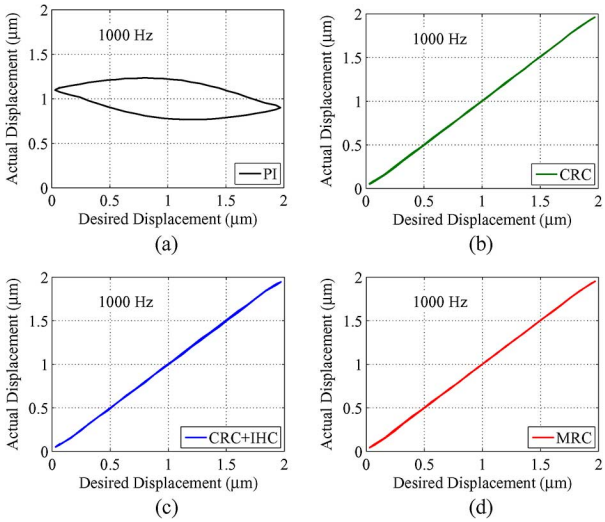

Fig. 10. Experimental results of the relations between actual displacements and the desired ones under 1000-Hz triangular reference input using (a) PI control, (b) CRC, (c) CRC+IHC, and (d) MRC, respectively.

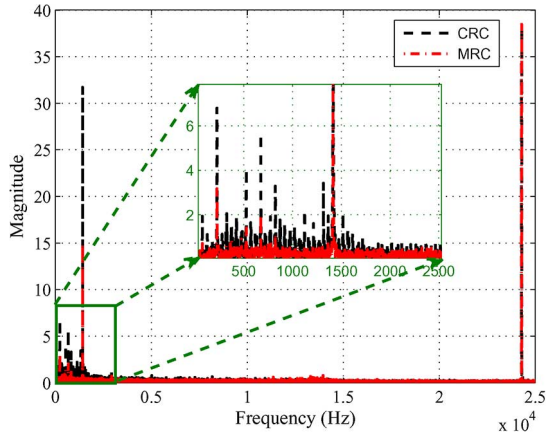

Fig. 11. Spectra of tracking error under 50-Hz triangular trajectory using CRC and MRC, respectively.

It can be seen from Fig. 9(b) that the introduction of IHC increases the rate that tracking errors converge, which coincides with experimental results in the reported works of RC+IHC such as [23] and [26]. However, from the detail of steady-state tracking error, as shown in Fig. 9(c), it can be observed that the MRC-based control approach shows better tracking accuracy as compared to the CRC+IHC, which is further validated in Table I. Such steady-state tracking performance improvement is quite important in the nanopositioning applications. For instance, in SPM-probe-based nanofabrication, the position error of the probe can directly affects the resulting nanofeatures and even variations in a few nanometers of the probe position can drastically affect the size and spacing of the nanofeatures [22]. On the other hand, the proposed MRC-based control approach provides a more convenient approach for practical applications without constructing the hysteresis model and its inversion.

Moreover, from the comparison of the experimental results with the CRC and CRC+IHC, we notice that the IHC has little influence on the steady-state tracking errors in terms of $e_{\max}$ and e_{rms}. The reasons could be: i) for periodic reference inputs, the hysteresis nonlinearity can be decomposed as a periodic disturbance, as theoretically analyzed in Section II-A. In fact, one of the advantages of the repetitive control approach is well effective to mitigate such periodic disturbance; ii) in practical applications, depending on the selections of the hysteresis models and the identification algorithms, the identified hysteresis model cannot completely account for the real hysteresis effect, which introduces the unavoidable inverse compensation error.

2) Hysteresis Compensation: To verify the effectiveness of the developed MRC on the hysteresis compensation, the relations between the actual displacements and the desired ones in the tracking performance tests are investigated. Since the piezo-actuated stage shows severer hysteresis nonlinearity at 1000 Hz than 50 and 500 Hz, as depicted in Fig. 8, the experimental results under 1000-Hz triangular trajectory are shown in Fig. 10 as an illustration for the evaluation of hysteresis compensation. It can be seen from the figure that the experimental results with PI control still show severe nonlinear effect. By contrast, the hysteresis nonlinearity can be effectively mitigated with the CRC, CRC+IHC, and MRC. From the quantitative comparison as listed in Table I, the MRC-based control approach shows better performance than CRC and CRC+IHC. Besides, the MRC avoids the constructions of IHC as compared to CRC+IHC, and it is also superior to CRC in disturbance rejection which will be experimentally validated in the next section.

C. Disturbance Rejection

As has been analyzed in Sections II-B and III-D, in principle, the MRC tends to have a better nonperiodic disturbance rejection capability than the CRC. To verify this, experiments are carried out with the ambient noise and one-time disturbance. The ambient noise is unavoidable in the practical applications and is generally nonperiodic. The one-time disturbance, i.e. the impulse noise, is also a common nonperiodic disturbance in experiments, which is usually investigated in the repetitive control systems [20].

By analyzing the ambient noise during the disturbance rejection experiments in the frequency domain, it is found that the ambient noise mainly occurs in the frequency range of 0–800 Hz. Hence, tracking error under 50-Hz triangular trajectory can well reflect the different disturbance rejection capabilities of MRC and CRC [19], [23], [24]. For evaluation, Fig. 11 shows the spectra of tracking error under 50-Hz triangular trajectory. As can be seen that the MRC exhibits superiority to CRC in the ambient disturbance rejection, which is owing to the fact that the MRC alleviates the nonperiodic disturbance amplification problem of CRC. This is also the reason why the MRC shows better tracking performance than CRC in the time domain as in Section IV-B.

To evaluate the one-time disturbance rejection capabilities of MRC and CRC, impulse signals are used as the one-time disturbances. The impulse signals perturb the system when the stage is tracking a 500-Hz triangular trajectory and achieves steady-state tracking error. Fig. 12(a) shows the responses to the input disturbance ($d_i(k)$ in Fig. 2), and Fig. 12(b) shows the responses to the output disturbance ($d_o(k)$ in Fig. 2). It can be seen from Fig. 12 that it takes much less time (at least two periods less) for MRC, as compared to the CRC, to reject the input/output one-time disturbance and achieve the steady

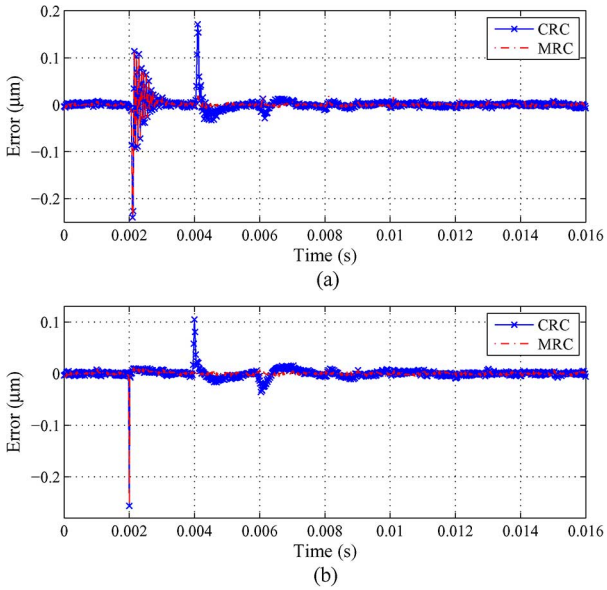

Fig. 12. Comparison of one-time disturbance rejection of MRC and CRC: (a) input one-time disturbance and (b) output one-time disturbance.

state, which demonstrates the better one-time disturbance rejection capability of MRC. It can also be observed from the figure that, after the impulse signals perturb the system with the CRC, several large error peaks appear before they decay to steady state. This is caused by the nonperiodic disturbance amplification problem of the CRC. By contrast, it can be seen from the Fig. 12 that the MRC alleviates such an issue.

V. Conclusion

In this paper, a MRC-based control approach is developed for the high-speed tracking of piezo-actuated nanopositioning stages with periodic reference inputs. First, the hysteresis nonlinearity is decomposed as a bounded periodic disturbance over a linear system. Then, the MRC strategy is developed which can directly mitigate the hysteresis nonlinearity by rejecting the periodic disturbance. Hence, the constructions of the hysteresis model and its inversion are avoided, which significantly reduces the implementation complexity as compared to the CRC-based control approaches with IHCs. Moreover, with the employment of a spectrum-selection filter, the MRC improves loop-shaping properties and thus alleviates the nonperiodic disturbance amplification problem of the CRC. The effectiveness of the developed control approach is verified on a piezo-actuated nanopositioning stage. Experimental results demonstrate that the MRC improves the tracking performance as compared to the PI control, CRC, and CRC+IHC. With the developed MRC strategy, the hysteresis nonlinearity under triangular reference up to 1000 Hz is well compensated. Besides, it is validated that the MRC has better nonperiodic disturbance rejection capability as compared to CRC.

References

[1] S. M. Salapaka and M. V. Salapaka, "Scanning probe microscopy," *IEEE Control Syst. Mag.*, vol. 28, no. 2, pp. 65–83, Apr. 2008.

[2] Y. L. Tian, D. W. Zhang, and B. Shirinzadeh, "Dynamic modelling of a flexure-based mechanism for ultra-precision grinding operation," *Presicion Eng.*, vol. 35, no. 4, pp. 554–565, 2011.

[3] U. Bhagat, B. Shirinzadeh, Y. L. Tian, and D. W. Zhang, "Experimental analysis of laser interferometry-based robust motion tracking control of a flexure-based mechanism," *IEEE Trans. Autom. Sci. Eng.*, vol. 10, no. 2, pp. 267–275, Apr. 2013.

[4] G. M. Clayton, S. Tien, K. K. Leang, Q. Z. Zou, and S. Devasia, "A review of feedforward control approaches in nanopositioning for high-speed SPM," *ASME J. Dyn. Syst., Meas., Control*, vol. 131, no. 6, p. 061101, 2009.

[5] G. Schitter, K. J. Astrom, B. E. DeMartini, P. J. Thurner, K. L. Turner, and P. K. Hansma, "Design and modeling of a high-speed AFM-scanner," *IEEE Trans. Contr. Syst. Technol.*, vol. 15, no. 5, pp. 906–915, Sep. 2007.

[6] S. Polit and J. Y. Dong, "Development of a high-bandwidth XY nanopositioning stage for high-rate micro-/nanomanufacturing," *IEEE/ASME Trans. Mechatron.*, vol. 16, no. 4, pp. 724–733, Aug. 2011.

[7] Y. M. Li, J. M. Huang, and H. Tang, "A compliant parallel XY micromotion stage with complete kinematic decoupling," *IEEE Trans. Autom. Sci. Eng.*, vol. 9, no. 3, pp. 538–553, Jul. 2012.

[8] S. Devasia, E. Eleftheriou, and S. O. R. Moheimani, "A survey of control issues in nanopositioning," *IEEE Trans. Control Syst. Technol.*, vol. 15, no. 5, pp. 802–823, Sep. 2007.

[9] A. J. Fleming and K. K. Leang, *Design, Modeling and Control of Nanopositioning Systems*. London, U.K.: Springer, 2014.

[10] A. J. Fleming and K. K. Leang, "Charge drives for scanning probe microscope positioning stages," *Ultramicroscopy*, vol. 108, no. 12, pp. 1551–1557, 2008.

[11] M. Rakotondrabe, "Bouc-Wen modeling and inverse multiplicative structure to compensate hysteresis nonlinearity in piezoelectric actuators," *IEEE Trans. Autom. Sci. Eng.*, vol. 8, no. 2, pp. 428–431, Apr. 2011.

[12] H. C. Liaw and B. Shirinzadeh, "Constrained motion tracking control of piezo-actuated flexure-based four-bar mechanisms for micro/nano manipulation," *IEEE Trans. Autom. Sci. Eng.*, vol. 7, no. 3, pp. 699–705, Jul. 2010.

[13] M. Rakotondrabe, K. Rabenorosoa, J. Agnus, and N. Chaillet, "Robust feedforward-feedback control of a nonlinear and oscillating 2-DOF piezocantilever," *IEEE Trans. Autom. Sci. Eng.*, vol. 8, no. 3, pp. 506–519, Jul. 2011.

[14] A. J. Fleming, S. Aphale, and S. O. R. Moheimani, "A new method for robust damping and tracking control of scanning probe microscope positioning stages," *IEEE Trans. Nanotechnol.*, vol. 9, no. 4, pp. 438–448, Jul. 2010.

[15] A. J. Fleming, "Nanopositioning system with force feedback for highperformance tracking and vibration control," *IEEE/ASME Trans. Mechatron.*, vol. 15, no. 3, pp. 433–447, Jun. 2010.

[16] Y. Wu and Q. Z. Zou, "Iterative control approach to compensate for both the hysteresis and the dynamics effects of piezo actuators," *IEEE Trans. Control Syst. Technol.*, vol. 15, no. 5, pp. 936–944, Sep. 2007.

[17] Y. K. Yong, S. O. R. Moheimani, B. J. Kenton, and K. K. Leang, "Invited review article: High-speed flexure-guided nanopositioning: Mechanical design and control issues," *Rev. Sci. Instrum.*, vol. 83, no. 12, p. 121101, 2012.

[18] U. Aridogan, Y. F. Shan, and K. K. Leang, "Design and analysis of discrete-time repetitive control for scanning probe microscopes," *ASME J. Dyn. Syst., Meas., Control*, vol. 131, no. 6, p. 061103, 2009.

[19] M. Tomizuka, T. C. Tsao, and K. K. Chew, "Analysis and synthesis of discrete-time repetitive controllers," *ASME J. Dyn. Syst., Meas., Control*, vol. 111, no. 3, pp. 353–358, 1989.

[20] G. S. Choi, Y. A. Lim, and G. H. Choi, "Tracking position control of piezoelectric actuators for periodic reference input," *Mechatronics*, vol. 12, no. 5, pp. 669–684, 2002.

[21] Q. S. Xu and Y. M. Li, "Dahl model-based hysteresis compensation and precise positioning control of an XY parallel micromanipulator with piezoelectric actuation," *ASME J. Dyn. Syst., Meas., Control*, vol. 132, no. 4, p. 041011, 2010.

[22] Y. F. Shan and K. K. Leang, "Dual-stage repetitive control with PrandtlC-Ishlinskii hysteresis inversion for piezo-based nanopositioning," *Mechatronics*, vol. 22, no. 3, pp. 271–281, 2012.

[23] C. Y. Lin and P. Y. Chen, "Precision tracking control of a biaxial piezo stage using repetitive control and double-feedforward compensation," *Mechatronics*, vol. 21, no. 1, pp. 239–249, 2011.

[24] Y. M. Li and Q. S. Xu, "Design and robust repetitive control of a new parallel-kinematic XY piezostage for micro/nanomanipulation," *IEEE/ASME Trans. Mechatron.*, vol. 17, no. 6, pp. 1120–1132, Dec. 2012.
[25] Y. R. Teo and A. J. Fleming, "A new repetitive control scheme based on non-causal FIR filters," in *Proc. Amer. Control Conf.*, Portland, OR, USA, Jun. 2014, pp. 991–996.
[26] Y. F. Shan and K. K. Leang, "Accounting for hysteresis in repetitive control design: Nanopositioning example," *Automatica*, vol. 48, no. 8, pp. 1751–1758, 2012.
[27] B. A. Francis and W. M. Wonham, "The internal model principle of control theory," *Automatica*, vol. 12, no. 5, pp. 457–465, 1976.
[28] X. Chen and M. Tomizuka, "New repetitive control with improved steady-state performance and accelerated transient," *IEEE Trans. Control Syst. Technol.*, vol. 22, no. 2, pp. 664–675, Mar. 2014.
[29] J. G. Yi, S. Chang, and Y. T. Shen, "Disturbance-observer-based hysteresis compensation for piezoelectric actuators," *IEEE/ASME Trans. Mechatron.*, vol. 14, no. 4, pp. 456–464, Aug. 2009.
[30] M. Tomizuka, "Zero phase error tracking algorithm for digital control," *ASME J. Dyn. Syst., Meas., Control*, vol. 109, no. 1, pp. 65–68, 1987.
[31] Q. S. Xu and Y. M. Li, "Model predictive discrete-time sliding mode control of a nanopositioning piezostage without modeling hysteresis," *IEEE Trans. Control Syst. Technol.*, vol. 20, no. 4, pp. 983–994, Jul. 2012.
[32] Habibullah, H. R. Pota, I. R. Petersen, and M. S. Rana, "Creep, hysteresis, cross-coupling reduction in the high-precision positioning of the piezoelectric scanner stage of an atomic force microscope," *IEEE Trans. Nanotechnol.*, vol. 12, no. 6, pp. 1125–1134, Nov. 2013.
[33] C. A. Desoer and M. Vidyasagar, *Feedback Systems: Input-Output Properties*. New York, NY, USA: Academic, 1975.
[34] C. X. Li, G. Y. Gu, M. J. Yang, and L. M. Zhu, "Design, analysis and testing of a parallel-kinematic high-bandwidth XY nanopositioning stage," *Rev. Sci. Instrum.*, vol. 84, no. 12, p. 125111, 2013.
[35] G. Y. Gu, M. J. Yang, and L. M. Zhu, "Real-time inverse hysteresis compensation of piezoelectric actuators with a modified Prandtl-Ishlinskii model," *Rev. Sci. Instrum.*, vol. 83, p. 065106, 2012.

Chun-Xia Li (S'12) received the B.E. (Hons.) degree in mechanical engineering from Shanghai Jiao Tong University, Shanghai, China, in 2011, where she is currently working toward the Ph.D. degree in mechanical engineering.

Her research interests include compliant mechanisms, design and control of high-bandwidth nanopositioning stages.

Miss Li was the recipient of the National Scholarship for Excellent Master Student granted by the Ministry of Education of China in 2012.

Guo-Ying Gu (S'10–M'13) received the B.E. (Hons.) degree in electronic science and technology and Ph.D. (Hons.) degree in mechatronic engineering from Shanghai Jiao Tong University, Shanghai, China, in 2006 and 2012, respectively.

From October 2010 to March 2011 and from November 2011 to March 2012, he was a Visiting Researcher with Concordia University, Montreal, QC, Canada. Since October 2012, he has been with Shanghai Jiao Tong University, where he is currently a Lecturer with the Faculty of the School of Mechanical Engineering. Supported by the Alexander von Humboldt Foundation, he was with the University of Oldenburg, Oldenburg, Germany, from August 2013 to July 2014. He has authored and coauthored more than 30 peer reviewed papers, including 20 SCI-indexed journal papers. He has served as the Guest Editor of the Special Issue on Micro/Nano Mechatronics and Automation in the *International Journal of Advanced Robotic Systems*. His research interests include robotics and equipment automation, design and high-bandwidth control of nanopositioning stages, modeling and control of systems involving with hysteresis.

Dr. Gu was the recipient of the Best Conference Paper Award at the 2011 IEEE International Conference on Information and Automation, Scholarship Award for Excellent Doctoral Student granted by the Ministry of Education of China in 2011, Hiwin Excellent Mechanical Doctoral Dissertation Award of China in 2013, and the Alexander von Humboldt Fellowship in 2013. He has served for several conferences as an international program committee member.

Mei-Ju Yang (S'12) received the B.E. degree in mechanical engineering from Shanghai Jiao Tong University, Shanghai, China, in 2009, where she is currently working toward the Ph.D. degree in mechanical engineering.

Her research interests include mechatronics, modeling and control of nanopositioning stages.

Miss Yang was the recipient of the National Scholarship for Excellent Doctoral Student granted by the Ministry of Education of China, in 2013 and in 2014, respectively.

Li-Min Zhu (M'12) received the B.E. (Hons.) degree and Ph.D. degree in mechanical engineering from Southeast University, Nanjing, China, in 1994 and 1999, respectively. From November 1999 to January 2002, he was a Postdoctoral Fellow with the Huazhong University of Science and Technology, Wuhan, China. Since March 2002, he has been with Shanghai Jiao Tong University, Shanghai, China, where he is currently a "Cheung Kong" Chair Professor and Vice Director of the State Key Laboratory of Mechanical System and Vibration. His research interests include fixturing, CNC machining, and 3-D measurement of complex shaped parts and control, sensing, and instrumentation for micro/nano manufacturing. He has published one monograph and more than 180 peer reviewed papers, including 105 on international journals.

Dr. Zhu was the recipient of the National Distinguished Youth Scientific Fund of China in 2013. He is an Associate Editor for the IEEE TRANSACTIONS ON AUTOMATION SCIENCE AND ENGINEERING and an Editorial Board Member of the *Proceedings of the IMechE, Part B: Journal of Engineering Manufacture*.